BIOCHEMISTRY

 Volume 45, Number 30 August 1, 2006

*Articles*

# A FAAH-Regulated Class of *N*-Acyl Taurines That Activates TRP Ion Channels†

Alan Saghatelian, Michele K. McKinney, Michael Bandell, Ardem Patapoutian, and Benjamin F. Cravatt*

*Departments of Cell Biology and Chemistry, The Skaggs Institute for Chemical Biology, The Scripps Research Institute, 10550 North Torrey Pines Road, La Jolla, California 92037*

*Received April 24, 2006; Revised Manuscript Received June 1, 2006*

ABSTRACT: Fatty acid amide hydrolase (FAAH) is an integral membrane enzyme that catabolizes several bioactive lipids in vivo. Most of the physiological substrates of FAAH characterized to date belong to the *N*-acyl ethanolamine (NAE) class of fatty acid amides, including the endocannabinoid anandamide, the anti-inflammatory lipid *N*-palmitoyl ethanolamine, and the satiating factor *N*-oleoyl ethanolamine. We recently identified a second structural class of fatty acid amides regulated by FAAH in vivo: the *N*-acyl taurines (NATs). Global metabolite profiling revealed high concentrations of long chain (≥C20) saturated NATs in the central nervous system (CNS) of FAAH(−/−) mice. Here, we use metabolite profiling to characterize the FAAH−NAT system in peripheral mouse tissues. Livers and kidneys of FAAH(−/−) mice possessed dramatic elevations in NATs, which, in contrast to those detected in the CNS, were enriched in polyunsaturated acyl chains (e.g., C20:4, C22:6). Peripheral NATs rose more than 10-fold within 1 h following pharmacological inactivation of FAAH and reached levels up to ∼5000 pmol/g tissue (C22:6 in kidney), implicating a constitutive and highly active pathway for NAT metabolism in which FAAH plays an integral part. Interestingly, NATs were found to activate multiple members of the transient receptor potential (TRP) family of calcium channels, including TRPV1 and TRPV4, which are both expressed in kidney. The dramatic elevation in endogenous levels of NATs following acute or chronic inactivation of FAAH, in conjunction with the pharmacological effects of these lipids on TRP channels, suggests the existence of a second major lipid signaling system regulated by FAAH in vivo.

Once viewed primarily as structural constituents of cell membranes, lipids are now recognized to also serve valuable signaling functions in vivo. Like other chemical transmitters, lipids bind and activate specific protein receptors to produce their biological effects (*1*, *2*). On the other hand, the hydrophobicity of lipids endows them with a unique set of properties relative to aqueous-soluble small molecules, including the ability to freely traverse the membrane compartments of cells and tissues. This latter feature designates metabolic enzymes with the primary responsibility of regulating the magnitude and duration of lipid signals in vivo.

The fatty acid amide family of lipid transmitters, which includes the endogenous cannabinoid anandamide [C20:4

† This work was supported by the National Institutes of Health Grants DA015197 (B.F.C.), DA017259 (B.F.C.), and NS046303 (A.P.), the Ruth L. Kirschstein NRSA Predoctoral Fellowship DA019425 (M.K.M.), a Burroughs Wellcome Fund Career Award (A.S.), an American Heart Association postdoctoral fellowship (M.B.), the Skaggs Institute for Chemical Biology, and the Helen L. Dorris Institute for the Study of Neurological and Psychiatric Disorders of Children and Adolescents.

* To whom correspondence should be addressed. Phone: (858) 784-8633. Fax: (858) 784-8023. E-mail: cravatt@scripps.edu.

[1] Abbreviations: NAE, *N*-acyl ethanolamine; FAAH, fatty acid amide hydrolase; DMP, discovery metabolite profiling; NAT, *N*-acyl taurine; TRP, transient receptor potential; HEPES, 4-(2-hydroxyethyl)-1-piperazineethanesulfonic acid; CNS, central nervous system; FFA, free fatty acid; ip, intraperitoneal; GPCR, G-protein coupled receptor.

10.1021/bi0608008 CCC: $33.50 
Published on Web 07/07/2006

*N*-acyl ethanolamine (NAE)[1] (*3*)], the sleep-inducing substance oleamide (*4*), the anti-inflammatory factor *N*-palmitoyl ethanolamine [C16:0 NAE; (*5*)], and the satiating signal *N*-oleoyl ethanoamine [C18:1 NAE; (*6*)], is regulated by the integral membrane enzyme fatty acid amide hydrolase (FAAH) (*7*). The genetic (*8*) or chemical (*9*) inactivation of FAAH leads to elevated endogenous levels of fatty acid amides and concomitant analgesic (*10*, *11*), anxiolytic (*9*), anti-depressant (*12*), sleep-enhancing (*13*), and anti-inflammatory (*10*, *14*, *15*) phenotypes, promoting FAAH as a potential therapeutic target for a range of nervous system and peripheral disorders (*16*). Prediction of the systems-wide impact of acute or chronic FAAH inhibition would benefit from an understanding of the full inventory of lipid metabolites regulated by this enzyme in vivo.

We recently introduced an untargeted liquid chromatography−mass spectrometry (LC−MS) method for characterizing the global metabolic effects of enzyme inactivation in vivo (*17*, *18*). We applied this approach, termed discovery metabolite profiling (DMP), to characterize nervous system tissues from FAAH(+/+) and (−/−) mice, resulting in the discovery of a novel structural class of endogenous FAAH substrates: the *N*-acyl taurines (NATs). NATs were elevated more than 10-fold in brains and spinal cords from FAAH(−/−) mice and were highly enriched in very long chain (≥C20) saturated acyl chains. These initial studies thus expanded our appreciation of the endogenous substrate portfolio of FAAH beyond the well-characterized NAEs and have raised several provocative questions. For instance, are NATs confined to the nervous system or do they exist in other tissues, and if so, are they also under the control of FAAH at these peripheral sites? Second, does the acute inactivation of FAAH by chemical inhibitors lead to elevations in the endogenous levels of NATs? Finally, are NATs biologically inert metabolites, or alternatively, might they serve as ligands for specific protein receptors? Here, we experimentally address each of these questions.

## EXPERIMENTAL PROCEDURES

*Tissue Isolation and Extraction.* A 2:1:1 solution of $CHCl_3$/MeOH/$H_2O$ (8 mL per tissue) was prepared for tissue extraction. For targeted LC measurements, standards were also included in this mixture. FAAH(−/−) and (+/+) mice (3−6 months of age) were sacrificed at the same time of day and tissues immediately isolated, weighed, placed into the $CHCl_3$/MeOH/$H_2O$ solution, and homogenized using dounce tissue grinders. Each sample was then centrifuged at 2500 rpm for 10 min at 4 °C in a glass vial. After centrifugation, the organic (bottom) and aqueous (top) layers were clearly distinguishable with a layer of insoluble material between them. The organic layer was carefully removed and transferred to another vial. The organic layer was concentrated under a stream of nitrogen and dissolved in 100 μL of $CHCl_3$ prior to analysis by LC−MS.

*Metabolite Analysis by LC−MS.* LC−MS analysis was performed using an Agilent 1100 MSD SL. For the LC analysis, a Gemini (Phenomenex) C18 column (5 μm, 4.6 × 100 mm) was used together with a precolumn (C18, 3.5 μm, 2 × 20 mm). Mobile phase A consisted of 95/5 water/methanol, and mobile phase B was made up of 60/35/5 2-propanol/methanol/water. Both A and B were supplemented with 0.1% ammonium hydroxide as solvent modifiers. The flow rate for each run started at 0.1 mL/min for 5 min, to alleviate the backpressure associated with injecting $CHCl_3$, followed by a flow rate of 0.4 mL/min for the duration of the gradient. The gradient started at 0% B and then linearly increased to 100% B over 60 min followed by an isocratic gradient of 100% B for 30 min before equilibrating for 10 min at 0% B. The total analysis time, including 5 min at 0.1 mL/min, was 105 min. MS analysis was performed with an electrospray source ionization (ESI) interface. The capillary voltage was set to 3.0 kV and the fragmentor voltage to 100 V. The drying gas temperature was 350 °C, the drying gas flow was 10 L/min, and the nebulizer pressure was 35 psi. For untargeted metabolite analysis (DMP), data was collected using a mass range of 200−1000 Da and each run was performed using 40 μL injections of tissue metabolite extract. The analysis of the resulting LC−MS data was performed with the program XCMS (http://metlin.scripps.edu) (*19*). Targeted metabolite analysis was performed by isotope-dilution MS using deuterated NAE and NAT standards, as described previously (*17*, *20*).

*Preparative HPLC Purification of NATs.* The metabolite extracts from five FAAH(−/−) livers were combined for a single LC purification using a Hitachi 7000 series HPLC. For the purification, a Gemini C18 column (5 μm, 10 × 50 mm) from Phenomenex was used. The mobile phase A consisted of 95/5 water/methanol/0.1% ammonium hydroxide, and mobile phase B was made up of 60/35/5 2-propanol/methanol/water/0.1% ammonium hydroxide. The gradient started at 0% B and then linearly increased to 100% B over 60 min followed by an isocratic gradient of 100% B for 20 min at a flow rate of 2.5 mL/min. Fractions (1 per minute) were collected using a Gilson FC 203B fraction collector. Fractions containing the *m*/*z* 410 and *m*/*z* 434 ions were identified by MS analysis. These fractions were then collected, and the solvent was removed using a rotary evaporator. The samples were then dissolved in a minimal amount of solvent B (200−300 μL) for exact mass and MS/MS analysis.

*Fourier Transform MS (FTMS) Analysis of NATs.* High accuracy measurements were performed in negative ion mode using a Bruker APEX III (7.0 T) FTMS (Billerica, MA) equipped with an Apollo electrospray source. The collected LC fractions were mixed with a collection of small molecule standards and directly infused at 3 μL/min using a Harvard Apparatus (Holliston, MA) syringe pump. Pneumatic assist at a backing pressure of 60 psi was used along with an optimized flow rate of heated counter-current drying gas (300 °C). Ion accumulation was performed using SideKick without pulsed gas trapping. Data acquisition times of approximately 1 min were used in broadband at the *m*/*z* range of 200−2200. Calculated molecular masses for ions generated by the mixture of small molecule standards were used to internally calibrate the data.

*Tandem MS Analysis of NATs.* MS/MS experiments were performed in negative ion mode using a Micromass QTof-*Micro* (Manchester, U.K.) equipped with a Z-spray electrospray source and a lockmass sprayer. The source temperature was set to 110 °C with a cone gas flow of 150 L/h, a desolvation gas temperature of 365 °C, and a nebulization gas flow of 350 L/h. The capillary voltage was set at 3.2 kV and the cone voltage at 30 V. Collision energy was set at

40−45 V. Samples were directly infused at 4 μL/min using a Harvard apparatus syringe pump (Holliston, MA). MS/MS data were collected in centroid mode over a scan range of 50−500 *m*/*z* for acquisition times of 2 min.

*Pharmacological Inhibtion of FAAH.* FAAH(+/+) mice were injected with URB597 (10 mg/kg, ip) or vehicle (saline/emulphor/ethanol, 18:1:1). At given times post-injection, tissue was isolated and processed as stated above. For 24 h experiments, URB-597 was injected every 4 h to maintain FAAH inhibition.

*Cellular Expression and Analysis of TRP Channels.* CHO cells were cultured in DMEM/F12 supplemented with 10% FBS. For expression of the TRP channels, the cells were transiently transfected (Fugene 6, Roche) with pcDNA5/FRT containing the ion channel cDNA and a yellow fluorescence reporter plasmid at a 3:1 ratio, to allow identification of transfected cells. Cells were plated in 24 well plates. Experiments were performed 2 days after transfection. Ratiometric calcium imaging of transiently transfected CHO cells was performed essentially as described (*21*). Briefly, cells were plated in 24 well plates, transiently transfected with the cDNA, and loaded with Fura-2 acetomethoxy ester according to manufacturer's protocol (Molecular Probes). After loading, the cells were washed with assay buffer (HEPES-buffered Hanks-balanced salt solution) and fluorescence was measured at excitation wavelengths alternating between 340 and 380 nm. Following subtraction of background fluorescence, the ratio of fluorescence at 340 and 380 nm was calculated. All graphs are averaged ratios of 20−40 individual cells. All experiments were performed at room temperature.

*Enzymatic Production of NATs*. In a glass vial were added taurine (4 μL, 0.5 M stock, final concentration 20 mM), tissue lysate (1 μg protein/μL final concentration), and PBS(pH 7.4) to a final volume of 99 μL. Heat-denatured samples were placed at 90 °C for 5 min and cooled to room temperature prior to the assay. The assay was initiated by the addition of arachidonoyl-CoA (1 μL, 10 mM stock in DMSO, final concentration 100 μM, Avanti Polar Lipids) followed by incubation for 60 min at 37 °C. The reaction was quenched with 0.5 N HCl (100 μL), and C18:1 NAT (1 uL, 2.5 mM stock in DMSO final concentration 25 μM) was added to the mixture as an internal standard. The lipids were extracted with a chloroform/methanol solution (2:1, 600 μL) and subseqeuently analyzed by LC−MS to measure the amount of 20:4 NAT produced. Additional reactions performed in the presence of the FAAH inhibitor URB597 (1 μM) confirmed that FAAH is not responsible for the enzymatic production of NATs (i.e., by potentially working in reverse).

## RESULTS

*DMP Analysis of Livers from FAAH(+/+) and (−/−) Mice*. In addition to the nervous system, FAAH is also expressed at high levels in several peripheral tissues in rodents, including liver, kidney, and testis (*7*, *14*). Of these peripheral tissues, the liver contains the highest quantity of FAAH activity, exceeding even the levels of FAAH observed in brain. We therefore elected to focus our DMP studies on liver tissues from FAAH(+/+) and (−/−) mice. Metabolite samples were prepared by organic extraction of freshly isolated and homogenized livers and subjected to untargeted LC−MS analysis as described in Experimental Procedures. Data analysis to identify differentially expressed metabolites in FAAH(+/+) and (−/−) tissues was carried out using the XCMS program (*19*), which computationally aligns and ratios the mass ion peaks observed in two LC−MS data sets and then rank-orders the observed differences based on statistical significance.

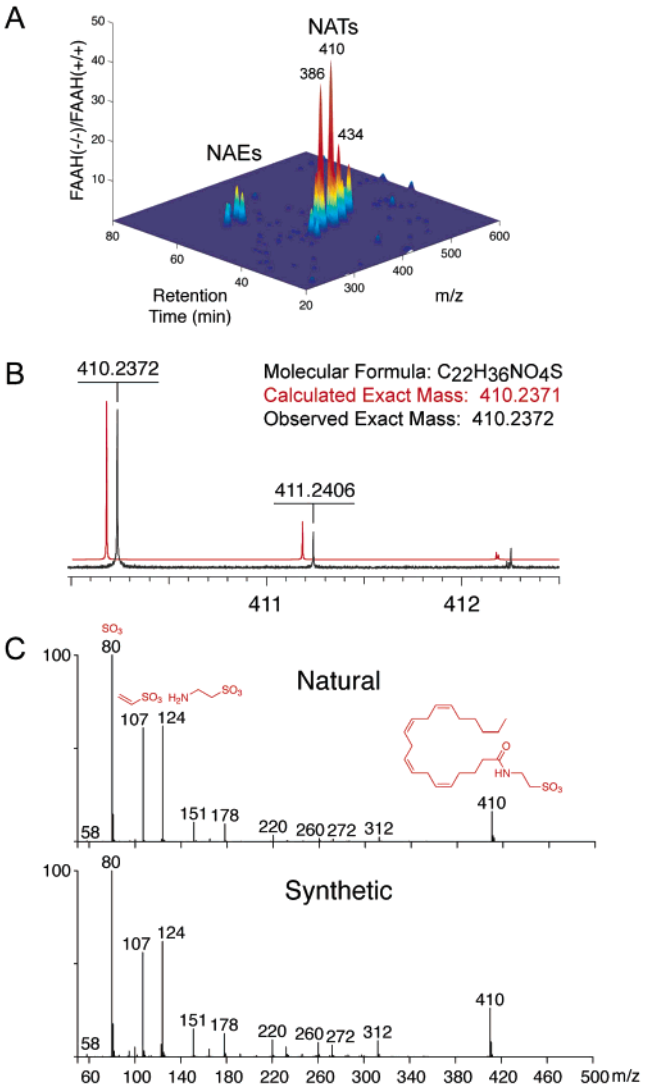


FIGURE 1: Discovery and characterization of polyunsaturated NATs. (A) Untargeted metabolite profiling of livers from FAAH(+/+) and (−/−) mice, plotted over a mass range of 200−600 and a retention time between 20 and 80 min, revealed a striking increase in the mass ion intensities ratios [(−/−)/(+/+)] of the NAT and NAE classes of lipids. Two of the largest changes within the NAT family belonged to metabolites with *m*/*z* values of 410 and 434. Further characterization of these metabolites by (B) ESI-FTMS and (C) MS/MS identified their structures as polyunsaturated NAT species containing C20:4 (*m*/*z* 410) and C22:6 (*m*/*z* 434) acyl chains (data only shown for C20:4 NAT). By extension, the *m*/*z* 386 metabolite was interpreted to represent C18:2 NAT.

Two major groups of lipid metabolites were elevated in livers of FAAH(−/−) mice which corresponded in mass and retention time to NAEs and NATs (Figure 1A and Table 1). Other common classes of lipids were unaltered in these tissues, including free fatty acids and phospholipids (Table 1). These data sets indicate that the role for FAAH in liver, as in the CNS, is primarily restricted to the catabolism of

Table 1: Relative Levels of Representative Lipids Measured by DMP in Liver Tissue from FAAH (+/+) and FAAH (−/−)[a]

| lipid class<br>acyl chain | FAAH(−/−)/FAAH(+/+)<br>liver |
|---|---|
| NAEs | |
| C16:0 | 6.4** |
| C18:1 | 8.6** |
| C18:0 | 3.9** |
| ceramides | |
| C16:0 | 1.2 |
| C18:1 | 1.4 |
| NATs | |
| C18:2 (386) | 37.0* |
| C18:1 (388) | 14.3* |
| C20:4 (410) | 42.0** |
| C22:6 (434) | 11.0* |
| phospholipids | |
| C34:1 PA | 0.6 |
| C36:2 PA | 0.7 |
| C34:1 PE | 0.9 |
| C36:3 PE | 0.9 |
| C36:2 PE | 0.6 |
| C36:2 PC | 0.8 |
| C36:2 PS | 0.7 |
| FFAs | |
| C16:0 | 0.9 |
| C18:1 | 0.9 |
| C18:0 | 0.9 |
| C20:4 | 1.4 |
| C22:6 | 1.1 |

[a] **, $p < 0.01$.

amidated lipids. Interestingly, however, the molecular masses of liver NATs differed considerably from those observed in the CNS (*17*). For example, two of the most intensely elevated NAT signals in FAAH(−/−) livers corresponded to the *m*/*z* ions 410 and 434 (Table 1), neither of which were elevated in the CNS of FAAH(−/−) mice. These masses matched those predicted for NATs bearing the polyunsaturated acyl chains C20:4 (arachidonoyl) and C22:6 (docosahexaenoyl), respectively. FTMS and MS/MS measurements of the *m*/*z* 410 ion verified these structural assignments (Figure 1B,C). Thus, despite performing a similar overall catabolic function in the CNS and liver, FAAH's specific substrate profile appeared to differ in these tissues. To further explore this premise, we compared the absolute levels of NATs in the CNS and peripheral tissues of FAAH(−/−) mice.

*Quantitation and Tissue Distribution of NATs.* We measured the absolute levels of NATs in FAAH(+/+) and (−/−) tissues by isotope-dilution MS (IDMS), where isotopically labeled standards are added to biological samples to enable ratiometric quantification of endogenous metabolites (*17*). In addition to providing estimates of the absolute concentrations of metabolites, IDMS exhibits increased sensitivity compared to DMP, owing to the measurement of mass ions in the targeted mode. We hoped that the enhanced sensitivity of IDMS would facilitate the characterization of NATs in FAAH(+/+) livers, where some of these lipids (e.g., C20:4 NAT) were too low in abundance for detection by DMP. Other peripheral tissues known to express high levels of FAAH (kidney and testis) were also evaluated to determine the anatomical distribution of NATs. IDMS experiments were performed using representative mono- and polyunsaturated $d_4$-NATs as internal standards ($d_4$-C18:1 NAT and $d_4$-C22:6 NAT, respectively).

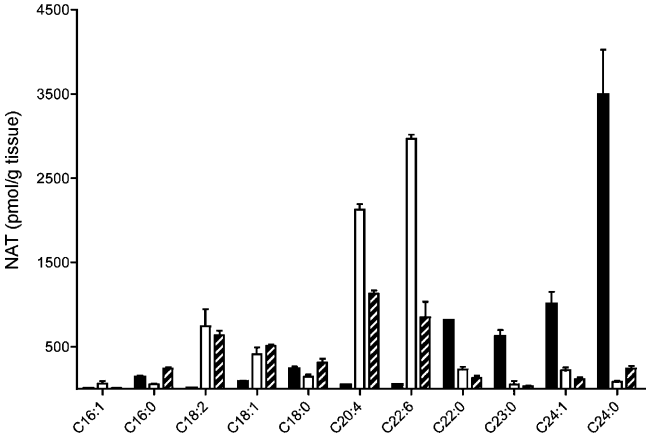


FIGURE 2: Absolute concentrations and acyl chain distribution of NATs in tissues from FAAH(−/−) mice. Measurement of the absolute levels of NATs was performed by targeted profiling [brain (black bars), liver (white bars), and kidney (hatched bars)]. Note that, although the distribution of FAAH-regulated NATs in both the CNS and periphery favors long acyl chains (≥ C20), their degrees of unsaturation vary dramatically. In the CNS, FAAH-regulated NATs are predominantly saturated, while these lipids are enriched in polyunsaturated chains in the liver and kidney.

NAT species with *N*-acyl chains ranging from C16 to C24 were identified in liver, kidney, and brain tissues (Figure 2), but not in testis (data not shown). The largest fold changes in NAT levels between FAAH(+/+) and (−/−) mice were observed in liver and corresponded to NATs bearing polyunsaturated acyl chains (C18:2, C20:4, C22:6) (Table 2). These polyunsaturated NATs were found at remarkably high levels in FAAH(−/−) mice, exceeding 2 nmol/g of tissue for the C20:4 and C22:6 NATs (Table 2). In contrast, concentrations of polyunsaturated NATs were at least 50-fold lower in FAAH(+/+) livers, where the C22:6 NAT was estimated at 50 pmol/g and the C20:4 NAT remained below the detection limit (20 pmol/g). Saturated and monounsaturated NATs were also elevated in FAAH(−/−) livers, but were present at lower absolute levels compared to polyunsaturated NATs (Table 2). Qualitatively similar results were obtained from kidney tissue, where NATs were elevated 3−37-fold in FAAH(−/−) samples with the highest absolute levels again being observed for polyunsaturated species (Table 2). In contrast to these peripheral tissues, FAAH(−/−) brains did not possess elevations in polyunsaturated NATs, instead being enriched exclusively in long chain saturated and monounsaturated NATs (Figure 2; also see ref *17*). The acyl chain distribution of NATs did not correlate with that of free fatty acids (FFAs) in either livers or brains of FAAH(−/−) mice (Figure 3), indicating that the distinct NAT profiles of these tissues were not simply due to differences in respective fatty acid composition.

*NAT Levels in Mice Treated with a FAAH Inhibitor.* The striking differences in acyl chain distribution of NATs from brains and livers/kidneys of FAAH(−/−) mice suggested distinct mechanisms for the production of these lipids in the CNS and periphery. To further examine this premise, we compared the accumulation of NATs in tissues from mice treated with the irreversible FAAH inhibitor URB597 (*9*).

Wild-type mice were administered URB597 (10 mg/kg, ip) or vehicle (saline/emulphor/ethanol 18:1:1) for specific times ranging from 60 min to 12 h, after which tissues were

Table 2: Absolute Concentrations (pmol/g) and Ratios of NATs in Liver and Kidney Tissues of FAAH(+/+) and (−/−)Mice (for All Data Shown, $p < 0.01$)

| | liver | | | kidney | | |
|---|---|---|---|---|---|---|
| | FAAH(−/−) (pmol/g) | FAAH(+/+) (pmol/g) | (−/−)/(+/+) | FAAH(−/−) (pmol/g) | FAAH(+/+) (pmol/g) | (−/−)/(+/+) |
| C18:2 | 741 | 18 | 41 | 632 | 59 | 11 |
| C18:1 | 408 | 22 | 19 | 510 | 109 | 5 |
| C18:0 | 141 | 20 | 7 | 311 | 92 | 3 |
| C20:4 | 2128 | 20 | 106 | 1130 | 157 | 7 |
| C22:6 | 2966 | 51 | 58 | 849 | 23 | 37 |
| C22:0 | 228 | 20 | 11 | 126 | 12 | 10 |
| C24:1 | 217 | 20 | 11 | 112 | 14 | 8 |
| C24:0 | 83 | 20 | 4 | 241 | 39 | 6 |

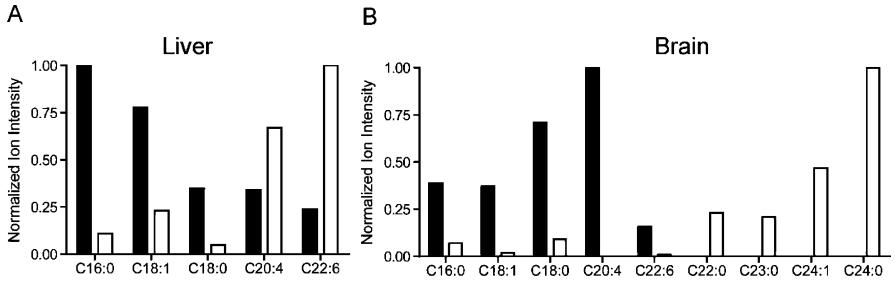


FIGURE 3: Normalized acyl chain distribution of free fatty acids [FFAs (black bars)] and NATs (white bars) in liver (A) and brain (B) tissue of FAAH(−/−) mice. Differences between the acyl chain profiles of FFAs and NATs in both the liver and brain indicate that the NAT distribution in these tissues is not simply correlated with their respective FFA concentrations.

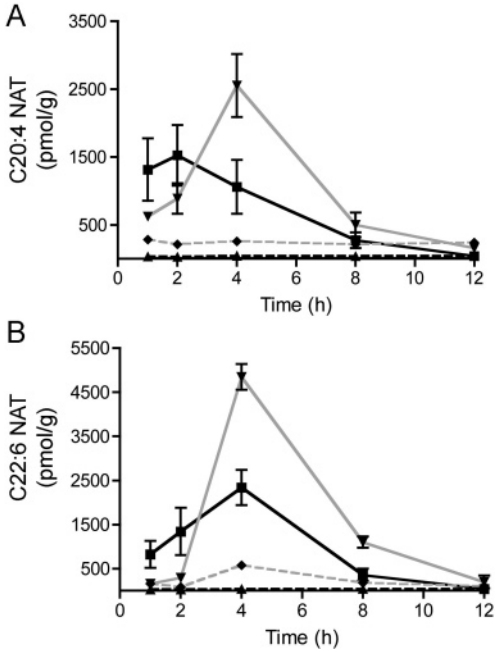


FIGURE 4: Acute inhibition of FAAH with URB597 (10 mg/kg, ip) leads to rapid accumulation of NATs in the liver (black lines with square symbols) and kidney (gray lines with inverted triangle symbols). Data are shown for 20:4 (A) and 22:6 (B) NATs. Mice treated with vehicle (18:1:1 saline/emulphor/ethanol) showed no change in their tissue NAT levels (liver, black dashed lines with triangle symbols; kidney, gray dashed lines with diamond symbols). Note that the peak NAT concentrations of inhibitor-treated mice reached and, in certain instances, even surpassed those found in FAAH(−/−) tissue (e.g., C22:6 NAT at 4 h).

harvested and NAT concentrations measured by IDMS. NAT levels escalated rapidly in liver and kidney, rising greater than 35-fold by 1 h following URB597 treatment compared to vehicle controls (Figure 4). Interestingly, peak concentrations of NATs observed at 2−4 h approached and, in certain cases, surpassed those observed in FAAH(−/−) tissues (e.g., 20:4 and 22:6 NAT in kidney). The remarkable rate and magnitude of accumulation of NATs in both livers and kidneys of mice following acute inactivation of FAAH indicates the presence of a tonically active pathway for the production of these lipids in peripheral tissues.

Table 3: Fold Increases in NAE and NAT Levels in Mouse Tissues Following Acute and Prolonged Inhibition of FAAH with URB597 (10 mg/kg, ip) Compared to Vehicle-Treated Controls

| | brain | | | liver | |
|---|---|---|---|---|---|
| | 2 h | 24 h[a] | | 2 h | 24 h[a] |
| | | NAEs | | | |
| C16:0 | 8.0** | 13.9** | C16:0 | 3.0 | ≥14*,[b] |
| C18:1 | 9.4** | 9.3* | C18:1 | 1.4 | ≥12** |
| C18:0 | 2.2 | 6.2** | C18:0 | 1.3 | ≥8** |
| | | NATs | | | |
| C22:0 | 1.2 | 2.1* | C18:1 | 33.9** | 20.9** |
| C24:1 | 1.2 | 2.6* | C20:4 | 98.6** | 89.1** |
| C24:0 | 1.0 | 1.7 | C22:6 | 28.2** | 73.9** |

[a] Prolonged inhibition for 24 h was achieved by administering URB597 every 4 h to maintain FAAH inactivation for the duration of the experiment. [b] Signals from vehicle-treated controls that fell below the MS detection limit ($5 \times 10^4$) resulted in fold-changes being reported as ≥ for these lipids. *, $p \leq 0.05$; **, $p \leq 0.01$.

In contrast, NAT levels in the CNS were largely unchanged at early time points (e.g., 2 h) following the acute inhibition of FAAH (Table 3). Extension of the time course to 24 h with repeated injections every 4 h to maintain FAAH inhibition revealed a modest, but significant increase in NATs in CNS tissues of URB597-treated mice (Table 3). As was observed previously in FAAH(−/−) mice (*17*), elevated NATs in the CNS contained saturated and monounsaturated, but not polyunsaturated, acyl chains. These results indicate that NATs in the CNS and periphery are not only distinguishable based on their acyl chain composition (saturated and polyunsaturated, respectively), but also on their rate of

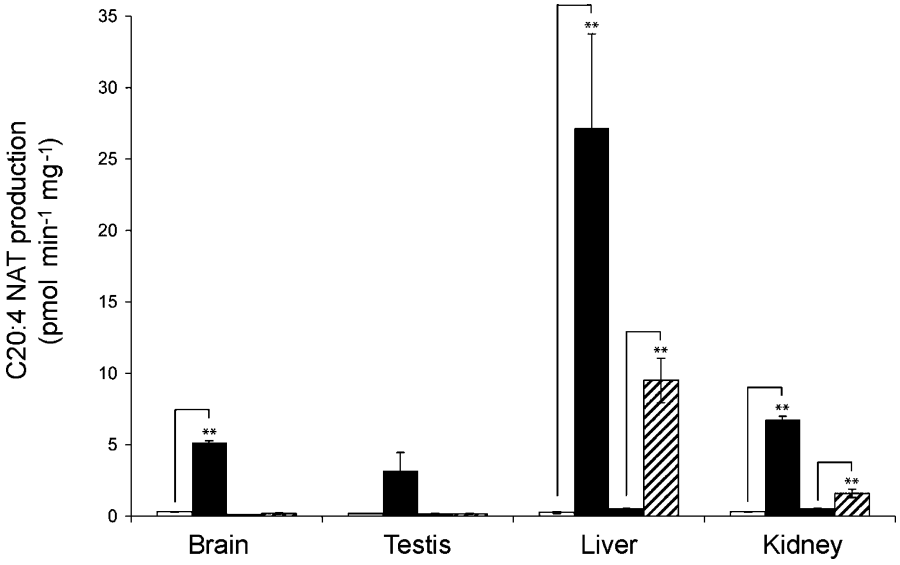


FIGURE 5: Evidence for a fatty acyl CoA:taurine *N*-acyltransferase activity in mouse tissues. Taurine (20 mM) and arachidonoyl-CoA (100 $\mu$M) were combined in the presence of tissue proteomes (100 $\mu$g, 1 $\mu$g/$\mu$L) and reacted for 1 h at 37 °C. Activities are shown for native membrane and soluble tissue fractions (black and hatched bars, respectively), as well as their respective heat-denatured controls (white and gray bars). Preincubation of tissue samples with URB597 (1 $\mu$M) did not affect the accumulation of NATs, indicating that FAAH does not participate in this process (data not shown).

accumulation following FAAH inactivation, which was slow in the CNS and rapid in the periphery.

*Evidence for an Enzymatic Pathway That Produces NATs.* The rapid accumulation of NATs in the liver and kidney of FAAH inhibitor-treated animals suggested an enzymatic pathway for the production of these lipids. Structurally related bile salts are biosynthesized by the enzyme bile acid coenzyme A (CoA):amino acid *N*-acyltransferase (BAT) that conjugates cholyl CoA to glycine or taurine (*22*). Consistent with a similar enzymatic pathway for the production of NATs, a heat-sensitive activity was detected in mouse tissue extracts for the formation of NATs from fatty acyl CoAs and taurine (Figure 5). This fatty acyl CoA:taurine *N*-acyltransferase activity was predominantly membrane-associated and most strongly expressed in liver, with lower levels also being detected in kidney, brain, and testis. On first glance, it is perhaps somewhat surprising that the levels of this enzyme activity were not higher in kidney, given that this organ possessed levels of NATs that were on par if not higher than liver following FAAH inactivation (Figure 4). A closer examination of the kinetics of NAT accumulation in liver and kidney revealed, however, a slight delay in the latter tissue (Figure 4). This intriguing finding might suggest that the major site of synthesis for NATs is the liver, with the accumulation of these lipids in kidney occurring primarily as a result of transport rather than de novo production at this organ site. Regardless, these data support the presence of an enzymatic pathway for NAT biosynthesis based on the conjugation of fatty acyl-CoAs and taurine in a process analogous to the generation of bile salts.

*NATs Activate Members of the TRPV Family of Cation Channels.* Lipids have been identified as ligands for multiple types of receptors, including G-protein-coupled receptors (GPCRs) (*1*, *2*), nuclear receptors (*23*), and ion channels (*24*). Fatty acid amides, in particular, have been shown to activate cannabinoid (CB) receptors (GPCRs) (*3*), peroxisome proliferation activated receptor alpha (PPARα) (nuclear receptor) (*25*), and members of the transient receptor potential (TRP) family of cation channels (*26*). Our initial pharmacological studies with NATs did not reveal any agonist activity for cannabinoid (GPCR) or nuclear receptors (e.g., PPARs) (data not shown). In contrast, NATs acted as excellent ligands for a subset of TRP channels. For example, 20:4 NAT activated both TRPV1 and TRPV4, but not TRPM8 (Figure 6A). Concentration-dependence profiles established $EC_{50}$ values of 21 $\mu$M (3−130 $\mu$M, 95% confidence limits) and 28 $\mu$M

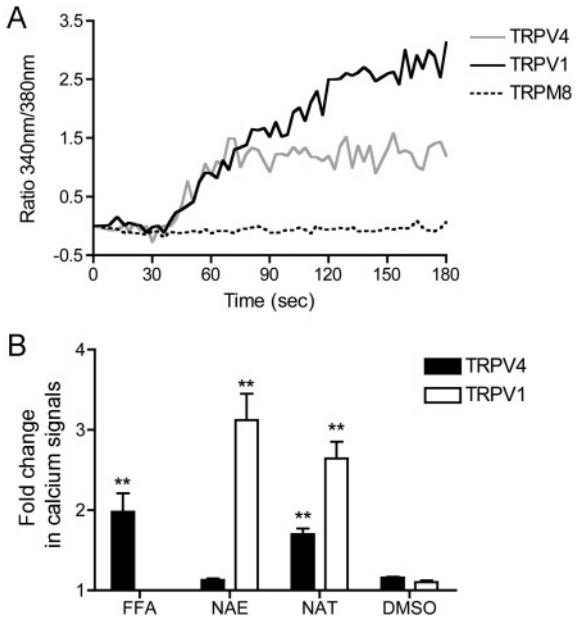


FIGURE 6: TRP channel activation by NATs. (A) 20:4 NAT was tested as an activator of the TRPV1 (black line), TRPV4 (gray line), and TRPM8 (black-dashed line) ion channels. Channel activation was measured using a Fura-2-based calcium-imaging assay as described in Experimental Procedures, where the ratio between the fluorescence at 340 and 380 nm is reflective of cellular calcium concentrations. (B) Activation of TRPV1 and TRPV4 by 20:4 FFA (arachidonic acid), 20:4 NAE (anandamine), and 20:4 NAT (lipids tested at 20 $\mu$M). Note that 20:4 NAT, but not 20:4 NAE, activated TRPV4. FFA was not tested with TRPV1. **, *p*-value ≤ 0.01 with respect to the DMSO control.

(11−70 $\mu$M, 95% confidence limits) for the activation of TRPV4 and TRPV1 by 20:4 NAT, respectively (see Supplementary Figure 1, Supporting Information). In the case of TRPV4, activity of 20:4 NAT was comparable to that of arachidonic acid and superior to that of anandamide, which did not affect TRPV4 (Figure 6B). Conversely, anandamide was a potent activator of TRPV1 ($EC_{50}$ value of 2.2 $\mu$M), as has been reported previously (*27*). Other NATs bearing saturated or monounsaturated acyl chains also stimulated TRPV4 (data not shown). These results suggest that the NAT−TRPV4 interaction depends on the negatively charged taurine headgroup, but accommodates a wide range of *N*-acyl chains. This latter observation raises the provocative possibility that NATs could act in concert to activate TRPV channels in vivo.

## DISCUSSION

Individual metabolic enzymes may possess multiple classes of endogenous substrates in vivo (*28*). The order of discovery of these substrates can unduly influence our view of the primary functions of enzymes. Untargeted profiling methods, like DMP (*17*, *18*), offer a powerful means to shed these historical biases and capture a more global view of the portfolio of physiological substrates of enzymes. Our current and previous DMP studies of FAAH offer an excellent case study that speaks to this point. Prior to this work, FAAH was recognized principally as a regulator of the NAE family of signaling lipids. The identification by DMP of NATs as a second class of lipids elevated in the CNS of FAAH(−/−) mice invoked biochemical functions for this enzyme that extended beyond the catabolism of NAEs. Here, we explored this premise further by characterizing NAT metabolism in a number of central and peripheral tissues from mice with acute (chemical) or chronic (genetic) disruption in FAAH activity. The resulting data sets confirm a key role for FAAH in controlling NAT levels in both the CNS and select peripheral tissues (e.g., liver, kidney), although some intriguing differences in these NAT pathways were illuminated.

The NATs regulated by FAAH in the CNS were highly enriched in long chain saturated and monounsaturated *N*-acyl chains that accumulated very slowly following acute FAAH inhibition by URB597. In contrast, pharmacological inactivation of FAAH led to a rapid elevation of polyunsaturated NATs in the liver and kidney. The extent to which FAAH exerts tonic control over these polyunsaturated NATs is perhaps best underscored by noting that the levels of these lipids rose from barely detectable (sub-20 pmol/g tissue) to concentrations that approximated, and in some cases surpassed, those observed in FAAH(−/−) tissues (~5000 pmol/g tissue) within 2 h following URB597. Interestingly, the rate and magnitude of accumulation of NATs in the liver and kidney of FAAH inhibitor-treated mice compared favorably to the elevation of NAEs in the CNS of these animals. Thus, inasmuch as these parameters reflect the physiological relevance of a substrate-enzyme pair, NATs may be regarded as equivalent in significance to NAEs when considering FAAH's endogenous functions.

Our data also argue for the existence of at least two distinguishable metabolic pathways for NAT production in vivo, one in the liver and kidney that displays high constitutive activity and a preference for polyunsaturated NATs, and a second in the CNS that is much slower and selective for saturated members of this lipid class. The rapid accumulation of polyunsaturated NATs in liver and kidney following URB597 treatment suggests further that these lipids are being tonically produced in the periphery, but under strict catabolic regulation by FAAH. Such endogenous metabolic tones established by a balance of biosynthetic and degradative enzyme activities are commonly invoked as a means of regulating lipid messengers (*29*), which cannot readily be stored in vesicles for controlled release. In these circuits, elevations in "lipid signaling tone" can be achieved by either increasing biosynthetic output or diminishing degradative activity. Although the identity of the enzyme(s) responsible for NAT biosynthesis remains unknown, high levels of an activity capable of biosynthesizing NATs from fatty acyl-CoA and taurine were detected in liver. Considering that the BAT enzyme responsible for bile salt production is also enriched in liver (*30*), it is possible that this enzyme may catalyze the formation of NATs. Consistent with this premise, human BAT has been shown to form *N*-acyl glycines when incubated with fatty acyl CoA substrates in vitro (*31*). Future studies with recombinant mouse BAT should clarify whether this enzyme can catalyze the conjugation of fatty acyl CoAs and taurine.

Evidence supporting a potential signaling function for NATs was obtained by screening these lipids against a panel of receptors and channels. Although NATs did not serve as ligands for the subset of GPCRs and nuclear hormone receptors tested in this study, they did activate multiple TRP channels (TRPV1, TRPV4) with a potency superior to NAEs in some cases. The activation of TRPV1 and TRPV4 by NATs is particularly intriguing given that both of these channels, like the NATs, are present in kidney, where they have been proposed to play roles in regulation of blood pressure and osmotic sensation (*32*, *33*). The $EC_{50}$ values for activation of TRPV1 and TPRV4 by C20:4 NAT were 28 and 21 $\mu$M, respectively. Interestingly, the aggregate estimated concentration of NATs in kidneys from FAAH inhibitor-treated animals exceeded 10 $\mu$M (assuming 1 g of tissue = 1 mL) suggesting that this family of lipids could achieve levels sufficient to activate TRPV channels in vivo (at least under conditions of FAAH inactivation). These findings suggest that further physiological studies of the FAAH−NAT−TRPV1/4 system in kidney are warranted. In this regard, it is noteworthy that FAAH inhibitors have been shown to reduce blood pressure in hypertensive rats (*34*). Although these antihypertensive effects were blocked by the CB1 receptor antagonist AM251, the additional participation of TRPV receptors cannot be excluded (especially considering that AM251 increased blood pressure independent of FAAH inactivation).

In summary, we have used metabolite profiling to bolster our understanding of the full inventory of biochemical functions performed by FAAH in vivo. The discovery of family of polyunsaturated NATs regulated by FAAH in liver and kidney suggests that this enzyme may regulate peripheral physiological events in addition to its recognized role as a terminator of endocannabinoid signaling in the CNS. In general support of this notion, inactivation of FAAH has been shown to modulate a number of peripheral processes, including blood pressure (*34*) and inflammation (*14*), and, at least in certain cases (*14*), these effects appear to be independent of CNS involvement. Finally, it is also provoca-

tive to consider the possibility that polyunsaturated NATs could serve as substrates for other metabolic enzymes, including cyclooxygenases (*35*) and lipoxygenases (*36*), which could produce NAT derivatives with unique signaling functions. Elucidating the contribution of NATs and their potential secondary metabolites to phenotypes observed in FAAH-inactivated animals will likely require experimental strategies to manipulate NAT tone without impacting other FAAH-regulated pathways (e.g., the NAE−endocannabinoid system). We describe in the accompanying paper (*37*) efforts toward achieving this goal in the form of an engineered FAAH mutant that shows a selective defect in the hydrolysis of NATs.

## ACKNOWLEDGMENT

We thank Sunia Trauger (FTMS measurements), Grace O'Maille (MS/MS) Aron Lichtman for assistance with cannabinoid receptor assays, and the Cravatt lab for helpful discussions and critical reading of the manuscript.

## SUPPORTING INFORMATION AVAILABLE

$EC_{50}$ determination of 20:4 NAT with TRPV4 and TRPV1; $EC_{50}$ determination of 20:4 NAE with TRPV1. This material is available free of charge via the Internet at http://pubs.acs.org.

## REFERENCES

1. Ishii, I., Fukushima, N., Ye, X., and Chun, J. (2004) Lysophospholipid receptors: signaling and biology, *Annu. Rev. Biochem. 73*, 321−354.
2. Di Marzo, V. (1998) Endocannabinoids and other fatty acid derivatives with cannabimimetic properties: biochemistry and possible physiopathological relevance, *Biochim. Biophys. Acta 1392*, 153−175.
3. Devane, W. A., Hanus, L., Breuer, A., Pertwee, R. G., Stevenson, L. A., Griffin, G., Gibson, D., Mandelbaum, A., Etinger, A., and Mechoulam, R. (1992) Isolation and structure of a brain constituent that binds to the cannabinoid receptor, *Science 258*, 1946−1949.
4. Cravatt, B. F., Prospero-Garcia, O., Siuzdak, G., Gilula, N. B., Henriksen, S. J., Boger, D. L., and Lerner, R. A. (1995) Chemical characterization of a family of brain lipids that induce sleep, *Science 268*, 1506−1509.
5. Lambert, D. M., Vandevoorde, S., Jonsson, K. O., and Fowler, C. J. (2002) The palmitoylethanolamide family: a new class of anti-inflammatory agents?, *Curr. Med. Chem. 9*, 663−674.
6. Rodriguez de Fonseca, F., Navarro, M., Gomez, R., Escuredo, L., Nava, F., Fu, J., Murillo-Rodriguez, E., Giuffrida, A., LoVerme, J., Gaetani, S., Kathuria, S., Gall, C., and Piomelli, D. (2001) An anorexic lipid mediator regulated by feeding, *Nature 414*, 209−212.
7. Cravatt, B. F., Giang, D. K., Mayfield, S. P., Boger, D. L., Lerner, R. A., and Gilula, N. B. (1996) Molecular characterization of an enzyme that degrades neuromodulatory fatty-acid amides, *Nature 384*, 83−87.
8. Cravatt, B. F., Demarest, K., Patricelli, M. P., Bracey, M. H., Giang, D. K., Martin, B. R., and Lichtman, A. H. (2001) Supersensitivity to anandamide and enhanced endogenous cannabinoid signaling in mice lacking fatty acid amide hydrolase, *Proc. Natl. Acad. Sci. U.S.A. 98*, 9371−9376.
9. Kathuria, S., Gaetani, S., Fegley, D., Valino, F., Duranti, A., Tontini, A., Mor, M., Tarzia, G., La Rana, G., Calignano, A., Giustino, A., Tattoli, M., Palmery, M., Cuomo, V., and Piomelli, D. (2003) Modulation of anxiety through blockade of anandamide hydrolysis, *Nat. Med. 9*, 76−81.
10. Lichtman, A. H., Shelton, C. C., Advani, T., and Cravatt, B. F. (2004) Mice lacking fatty acid amide hydrolase exhibit a cannabinoid receptor-mediated phenotypic hypoalgesia, *Pain 109*, 319−327.
11. Hohmann, A. G., Suplita, R. L., Bolton, N. M., Neely, M. H., Fegley, D., Mangieri, R., Krey, J. F., Walker, J. M., Holmes, P. V., Crystal, J. D., Duranti, A., Tontini, A., Mor, M., Tarzia, G., and Piomelli, D. (2005) An endocannabinoid mechanism for stress-induced analgesia, *Nature 435*, 1108−1112.
12. Gobbi, G., Bambico, F. R., Mangieri, R., Bortolato, M., Campolongo, P., Solinas, M., Cassano, T., Morgese, M. G., Debonnel, G., Duranti, A., Tontini, A., Tarzia, G., Mor, M., Trezza, V., Goldberg, S. R., Cuomo, V., and Piomelli, D. (2005) Antidepressant-like activity and modulation of brain monoaminergic transmission by blockade of anandamide hydrolysis, *Proc. Natl. Acad. Sci. U.S.A. 102*, 18620−18625.
13. Huitron-Resendiz, S., Sanchez-Alavez, M., Wills, D. N., Cravatt, B. F., and Henriksen, S. J. (2004) Characterization of the sleep-wake patterns in mice lacking fatty acid amide hydrolase, *Sleep 27*, 857−865.
14. Cravatt, B. F., Saghatelian, A., Hawkins, E. G., Clement, A. B., Bracey, M. H., and Lichtman, A. H. (2004) Functional disassociation of the central and peripheral fatty acid amide signaling systems, *Proc. Natl. Acad. Sci. U.S.A. 101*, 10821−10826.
15. Holt, S., Comelli, F., Costa, B., and Fowler, C. J. (2005) Inhibitors of fatty acid amide hydrolase reduce carrageenan-induced hind paw inflammation in pentobarbital-treated mice: comparison with indomethacin and possible involvement of cannabinoid receptors, *Br. J. Pharmacol. 146*, 467−476.
16. Cravatt, B. F., and Lichtman, A. H. (2003) Fatty acid amide hydrolase: an emerging therapeutic target in the endocannabinoid system, *Curr. Opin. Chem. Biol. 7*, 469−475.
17. Saghatelian, A., Trauger, S. A., Want, E. J., Hawkins, E. G., Siuzdak, G., and Cravatt, B. F. (2004) Assignment of endogenous substrates to enzymes by global metabolite profiling, *Biochemistry 43*, 14332−14339.
18. Saghatelian, A., and Cravatt, B. F. (2005) Global strategies to integrate the proteome and metabolome, *Curr. Opin. Chem. Biol. 9*, 62−68.
19. Smith, C. A., Want, E. J., O'Maille, G., Abagyan, R., and Siuzdak, G. (2006) XCMS: processing mass spectrometry data for metabolite profiling using nonlinear peak alignment, matching, and identification, *Anal. Chem. 78*, 779−787.
20. Clement, A. C., Hawkins, E. G., Lichtman, A. H., and Cravatt, B. F. (2003) Increased seizure susceptibility and pro-convulsant activity of anandamide in mice lacking fatty acid amide hydrolase, *J. Neurosci. 23*, 3916−3923.
21. Bandell, M., Dubin, A. E., Petrus, M. J., Orth, A., Mathur, J., Hwang, S. W., and Patapoutian, A. (2006) High-throughput random mutagenesis screen reveals TRPM8 residues specifically required for activation by menthol, *Nat. Neurosci. 9*, 493−500.
22. Shonsey, E. M., Sfakianos, M., Johnson, M., He, D., Falany, C. N., Falany, J., Merkler, D. J., and Barnes, S. (2005) Bile acid coenzyme A: amino acid N-acyltransferase in the amino acid conjugation of bile acids, *Methods Enzymol. 400*, 374−394.
23. Chawla, A., Repa, J. J., Evans, R. M., and Mangelsdorf, D. J. (2001) Nuclear receptors and lipid physiology: opening the X-files, *Science 294*, 1866−1870.
24. Benham, C. D., Davis, J. B., and Randall, A. D. (2002) Vanilloid and TRP channels: a family of lipid-gated cation channels, *Neuropharmacology 42*, 873−888.
25. Fu, J., Gaetani, S., Oveisi, F., Lo Verme, J., Serrano, A., Rodriguez De Fonseca, F., Rosengarth, A., Luecke, H., Di Giacomo, B., Tarzia, G., and Piomelli, D. (2003) Oleylethanolamide regulates feeding and body weight through activation of the nuclear receptor PPAR-alpha, *Nature 425*, 90−93.
26. Van Der Stelt, M., and Di Marzo, V. (2004) Endovanilloids. Putative endogenous ligands of transient receptor potential vanilloid 1 channels, *Eur. J. Biochem. 271*, 1827−1834.
27. Ross, R. A. (2003) Anandamide and vanilloid TRPV1 receptors, *Br. J. Pharmacol. 140*, 790−801.
28. Tipton, K. F., Boyce, S., O'Sullivan, J., Davey, G. P., and Healy, J. (2004) Monoamine oxidases: certainties and uncertainties, *Curr. Med. Chem. 11*, 1965−1982.
29. Bari, M., Battista, N., Fezza, F., Gasperi, V., and Maccarrone, M. (2006) New insights into endocannabinoid degradation and its therapeutic potential, *Mini-Rev. Med. Chem. 6*, 257−268.
30. Falany, C. N., Fortinberry, H., Leiter, E. H., and Barnes, S. (1997) Cloning, expression, and chromosomal localization of mouse liver bile acid CoA:amino acid N-acyltransferase, *J. Lipid Res. 38*, 1139−1148.
31. O'Byrne, J., Hunt, M. C., Rai, D. K., Saeki, M., and Alexson, S. E. (2003) The human bile acid-CoA:amino acid N-acyltransferase functions in the conjugation of fatty acids to glycine, *J. Biol. Chem. 278*, 34237−34244.

32. Liedtke, W., Choe, Y., Marti-Renom, M. A., Bell, A. M., Denis, C. S., Sali, A., Hudspeth, A. J., Friedman, J. M., and Heller, S. (2000) Vanilloid receptor-related osmotically activated channel (VR-OAC), a candidate vertebrate osmoreceptor, *Cell 103*, 525−535.
33. Wang, Y., and Wang, D. H. (2006) A novel mechanism contributing to development of Dahl salt-sensitive hypertension: role of the transient receptor potential vanilloid type 1, *Hypertension 47*, 609−614.
34. Batkai, S., Pacher, P., Osei-Hyiaman, D., Radaeva, S., Liu, J., Harvey-White, J., Offertaler, K., Mackie, K., Rudd, M. A., Bukoski, R. D., and Kunos, G. (2004) Endocannabinoids acting at CB1 receptors regulate cardiovascular function in hypertension, *Circulation 110*, 1996−2002.
35. Kozak, K. R., Crews, B. C., Morrow, J. D., Wang, L. H., Ma, Y. H., Weinander, R., Jakobsson, P. J., and Marnett, L. J. (2002) Metabolism of the endocannabinoids, 2-arachidonylglycerol and anandamide, into prostaglandin, thromboxane, and prostacyclin glycerol esters and ethanolamides, *J. Biol. Chem. 277*, 44877−44885.
36. Kozak, K. R., Gupta, R. A., Moody, J. S., Ji, C., Boeglin, W. E., DuBois, R. N., Brash, A. R., and Marnett, L. J. (2002) 15-Lipoxygenase metabolism of 2-arachidonylglycerol. Generation of a peroxisome proliferator-activated receptor alpha agonist, *J. Biol. Chem. 277*, 23278−23286.
37. McKinney, M. K., and Cravatt, B. F. (2006) Structure-based design of a FAAH variant that discriminates between the *N*-acyl ethanolamine and taurine families of signaling lipids, *Biochemistry, 45*, 9016−9022.

BI0608008